## Foundry-fabricated photonic integrated circuit for flex-grid entanglement distribution

Alexander Miloshevsky,<sup>1,†</sup> Hsuan-Hao Lu,<sup>1</sup> Lucas M. Cohen,<sup>2</sup> Karthik V. Myilswamy,<sup>2</sup> Saleha Fatema,<sup>2</sup> Muneer Alshowkan,<sup>1</sup> Andrew M. Weiner,<sup>2</sup> and Joseph M. Lukens<sup>1,3</sup>

<sup>1</sup>Quantum Information Science Section, Computational Sciences and Engineering Division,
Oak Ridge National Laboratory, Oak Ridge, Tennessee 37831, USA

<sup>2</sup>School of Electrical and Computer Engineering and Purdue Quantum Science and Engineering Institute,
Purdue University, West Lafayette, Indiana 47907, USA

<sup>3</sup>Research Technology Office and Quantum Collaborative, Arizona State University, Tempe, Arizona 85287, USA

†miloshevskya@ornl.gov

**Abstract:** We demonstrate a silicon photonic integrated circuit fabricated through the CMOS manufacturing process, which features a bidirectionally pumped microring to achieve over 116 high-fidelity polarization entangled channels covering the entire optical C+L-band for flex-grid entanglement distribution.

The forthcoming quantum internet [1] must possess adaptability for on-demand entanglement distribution among numerous end-users, accommodate varying user data needs, and navigate unforeseen disruptions in the network. Recent experiments combining broadband polarization entanglement with wavelength-selective switches (WSSs) show promise [2–4]. Leveraging concepts proven in classical "flex-grid" optical networking [5], the center wavelength, bandwidth, and lightpath of any quantum demand can be reconfigured adaptively and by request. Nevertheless, the need for broadband and compact polarization-entangled sources, compatible with CMOS and supporting ultradense channel spacings, remains unmet. In this work, we introduce a novel on-chip source which incorporates a bidirectionally pumped microring resonator (MRR) with integrated polarization splitter-rotators (PSRs), enabling efficient wavelength-multiplexed entanglement distribution for flex-grid networks. We validate high-fidelity operation through quantum state tomography (QST) of 116 channel pairs and adjacent frequency bin groupings, highlighting the potential for flexible bandwidth allocations of quantum resources on demand.

Utilizing AIM's process design kit and fabrication through their multi-project wafer service [6], our chip comprises a central MRR sandwiched between a pair of PSRs [Fig. 1(a)]. The first PSR spatially separates the pump light according to polarization—transverse electric (TE) or transverse magnetic (TM)—and rotates the TM portion to a TE output. Bidirectionally coupled into the MRR, the pump photons generate entangled photon pairs through spontaneous four-wave mixing in both directions. The generated signal and idler photons exhibit energy-time entanglement across multiple pairs of resonances defined by the MRR, with a free spectral range of 38.4 GHz and intrinsic (loaded) Q factors of  $3.7 \times 10^5$  ( $3.7 \times 10^4$ ). After extraction from the MRR, a second PSR converts one pathway back to TM polarization before recombining with the unrotated TE pathway. When the pair generation probabilities are balanced between the two counterpropagating processes, each pair of energy-matched resonances manifests a polarization Bell state  $|\Phi^+\rangle = \frac{\sqrt{1}}{2}(|H_{\omega_k}H_{\omega_{-k}}\rangle + |\Psi_{\omega_k}V_{\omega_{-k}}\rangle)$ , where the integer  $k \ge 1$  denotes the  $k^{th}$  frequency-bin pair (number of resonances away from the pump).

Figure 1(b) illustrates our experimental setup. We operate a tunable continuous-wave laser (Santec TSL-570) to pump the chip, aligning the pump wavelength with one of the ring resonances. We follow the laser with three dense wavelength division multiplexers (DWDMs): two 100 GHz passband and one 50 GHz passband, to attenuate the background noise in its spectrum. Then, a polarization controller (PC) manages the ratio of TE and TM polarization coupling (of ~10 dBm in total) into the chip. Upon exiting the chip, another set of three DWDMs, replicating the prior configuration, isolate the newly generated broadband entangled photons from the residual pump light. We implement a feedback loop in the pass channel of the first output DWDM to ensure the pump remains aligned with the intended cavity resonance to counter thermal drift. Finally, we employ a programmable pulse shaper (Finisar Waveshaper 4000B) as a WSS to route a pair of frequency bins, one from the signal side and one from the idler, to two separate optical fibers for subsequent state characterization. Two-qubit polarization QST is carried out using a pair of motorized polarization analyzers [7] followed by photon detection with superconducting nanowire

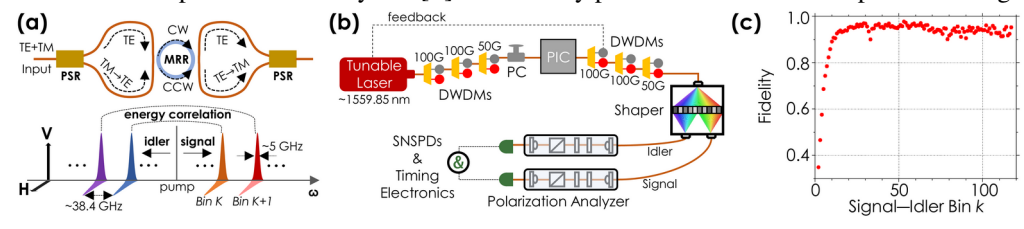


Fig. 1. (a) Schematic of photonic integrated circuit (top) for generation of wavelength-multiplexed polarization-entangled photons (bottom). (b) Experimental setup. (c) Fidelities from quantum state tomography of 116 energy-matched bins. See text for details.

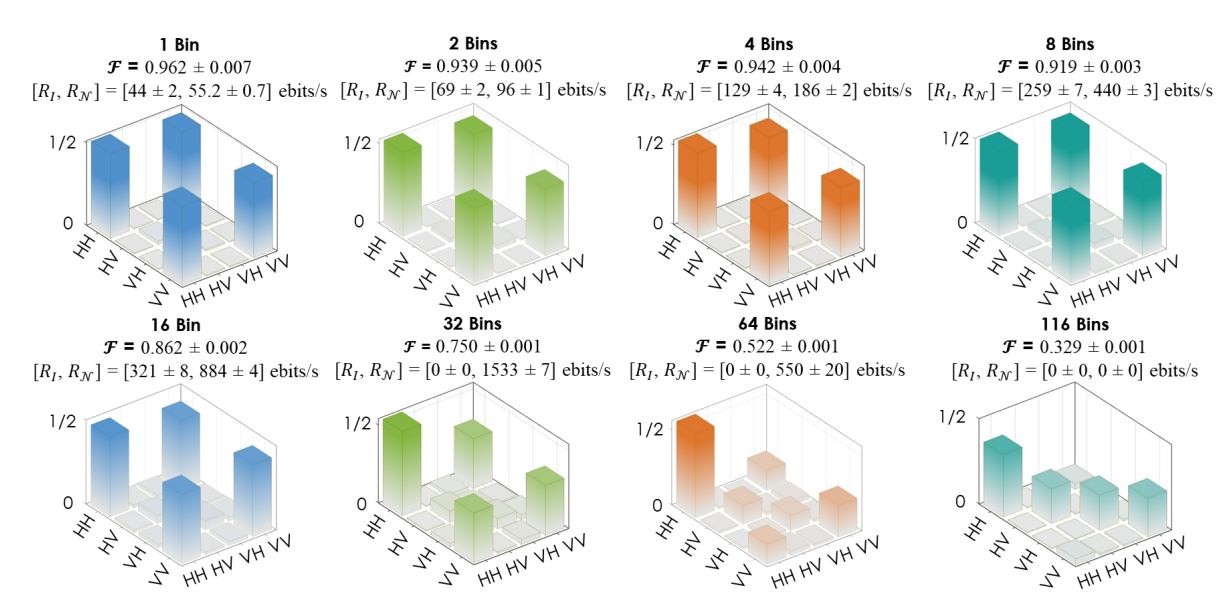


Fig. 2. Measured density matrix, fidelity, and the entangled bit rate for different bin groupings.

single-photon detectors (SNSPDs; Quantum Opus). For each bin pair, we scan through a total of 36 polarization projections, collecting coincidence counts (30 s per projection) for subsequent Bayesian inference [8, 9]. Density matrix samples from Markov chain Monte Carlo simulations enable the calculation of quantum state fidelity (with respect to  $|\Phi^+\rangle$ ) and other entanglement metrics. As expected, fidelities steadily improve as the separation with the residual pump increases [Fig. 1(c)] and plateau around 0.90 to 0.98, highlighting our ultrabroadband source as one of the highest-quality polarization-entangled sources in a fully on-chip design.

In a flex-grid configuration, when certain users seek additional bandwidth, we also have the flexibility to group adjacent bins together for reallocation, effectively enhancing the coincidence rate. However, such bandwidth expansion can easily decrease fidelity as well: the coincidence-to-accidental ratio generally reduces due to higher multipair-induced accidentals [10], and wider-bandwidth channels are more sensitive to any polarization-mode dispersion present in the optical fiber or components. Consequently, striking a balance between these competing factors—optimizing throughput while upholding entanglement quality above an application-specific threshold—emerges as a matter worth investigating. Figure 2 illustrates how bin grouping impacts state quality as evaluated through polarization QST. Our approach involves initially passing one bin on each side of the spectrum (k = 58) and symmetrically widening the filter passband, resulting in output states comprised of 2, 4, 8, 16, etc. consecutive frequency bins. As anticipated, state fidelity decreases with larger bin groupings, while the coincidence rate rises, a tradeoff which we can quantify through the entangled bit rate (EBR) defined as the distillable entanglement times the coincidence rate [7]. Lower and upper bounds on EBR (ebits/s), [ $R_I$ ,  $R_N$ ], can be obtained from the coherent information  $R_I$  and log-negativity  $R_N$ , respectively. In general, EBR increases as bins are grouped together due to the rising flux but eventually decreases as the polarization state becomes increasingly mixed. These findings show the flexibility of our compact design to adapt to end-user demands and varying channel conditions.

This work was performed in part at Oak Ridge National Laboratory, operated by UT-Battelle for the U.S. Department of Energy under contract no. DE-AC05-00OR22725. The Quantum Collaborative, led by Arizona State University, provided valuable expertise and resources for this work. Funding was provided by the U.S. Department of Energy, Office of Science, Advanced Scientific Computing Research (ERKJ353, ERKJ378) and the National Science Foundation (ECCS-2034019).

## References

- 1. S. Wehner, D. Elkouss, and R. Hanson, Science 362, eaam9288 (2018).
- 2. N. B. Lingaraju, H.-H. Lu, S.Seshadri, D. E. Leaird, A. M. Weiner, and J. M. Lukens, Optica 8, 329 (2021).
- 3. F. Appas, F. Baboux, M. I. Amanti, A. Lemaítre, F. Boitier, E. Diamanti, and S. Ducci, npj Quantum Inf. 7, 118 (2021).
- 4. M. Alshowkan, B. P. Williams, P. G. Evans, N. S. Rao, E. M. Simmerman, H.-H. Lu, N. B. Lingaraju, A. M. Weiner, C. E. Marvinney, Y.-Y. Pai, B. J. Lawrie, N. A. Peters, and J. M. Lukens, *PRX Quantum* 2, 040304 (2021).
- 5. O. Gerstel, M. Jinno, A. Lord, and S. J. Ben Yoo, IEEE Commun. Mag. 50, S12-S20 (2012).
- N. M. Fahrenkopf, C. McDonough, G. L. Leake, Z. Su, E. Timurdogan, and D. D. Coolbaugh, *IEEE J. Sel. Top. Quantum Electron.* 25, 8201406 (2019).
- 7. M. Alshowkan, J. M. Lukens, H.-H. Lu, B T. Kirby, B P. Williams, W P. Grice, and N. A. Peters, Opt. Lett. 47, 6480 (2022).
- 8. R. Blume-Kohout, New J. Phys. 12, 043034 (2010).
- 9. J. M. Lukens, K. J. H. Law, A. Jasra, and P. Lougovski, New J. Phys. 22, 063038 (2020).
- 10. J. Alnas, M. Alshowkan, N. S. V. Rao, N. A. Peters, and J. M. Lukens, Opt. Express 30, 24375 (2022).